



Investigation of the Influence of Subgrid-Scale Stress on the Accuracy of Non-intrusive Spatial Pressure Measurement using a DNS Channel Flow Database

Seth Siddle-Mitchell¹ and Xiaofeng Liu²
San Diego State University, San Diego, California, 92182-1308

and

Joseph Katz³
Johns Hopkins University, Baltimore, Maryland, 21218

The effect of the subgrid-scale (SGS) stress due to limited PIV resolution on pressure measurement accuracy is investigated using data from a direct numerical simulation of turbulent channel flow available at the John Hopkins University Turbulence Database (JHTDB). A series of 1400 consecutive realizations of sample block data with 512×512×49 grid nodal points were selected and spatially filtered with a 17×17×17 box average with a 50% planar overlap, giving rise to PIV resolution of roughly 62.6 times of the viscous length scale of the turbulent channel flow. Comparison of the reconstructed pressure at different levels of pressure gradient approximation with the filtered pressure shows that the neglect of the viscous term results in a small but noticeable change in the reconstructed pressure, especially in regions near the channel walls. As a contrast, the neglect of the SGS stress results in a more significant increase in both the bias and the random errors, indicating the SGS term *must* be accounted for in PIV pressure measurement. Correction using similarity SGS modeling reduces the random error due to omission of SGS stress from 106.3% to 80.4% of the r.m.s. fluctuation of the filtered pressure, confirming the benefit of the error compensation method.

Nomenclature

δ_{ij}	= the Kronecker delta for index notation
ν	= the molecular kinematic viscosity
ρ_0	= constant density for incompressible flow
τ_{ij}	= subgrid-scale stress
f	= forcing term in the direct numerical simulation
p	= kinematic pressure, i.e., pressure divided by constant density
\tilde{p}	= filtered kinematic pressure
t	= time
u_i	= the <i>i</i> -th velocity component using index notation
\tilde{u}_i	= filtered velocity component
v	= the wall-normal velocity at the top and bottom walls of the channel
x, y, z	= the streamwise, wall normal and spanwise directions of the channel flow
i, j	= index notation representing the <i>x, y, or z</i> components

¹ Graduate Research Assistant, Department of Aerospace Engineering, SDSU. AIAA Student Member.

² Assistant Professor, Department of Aerospace Engineering, SDSU. AIAA Associate Fellow.
 Email: Xiaofeng.Liu@mail.sdsu.edu.

³ Professor, Department of Mechanical Engineering, Johns Hopkins University. AIAA Senior Member.

I. Introduction

Knowledge of pressure distribution in flow field is of fundamental importance in many engineering applications. For example, pressure is responsible for aerodynamic or hydrodynamic forces such as lift and form drag acting on a moving body in fluid. Wall pressure fluctuations result in excitation of structures, leading to flow-induced vibrations and acoustic noise¹ (Blake 1986). In turbulence research, the pressure diffusion and the pressure-strain tensors are key unresolved parameters in turbulence modeling^{2,3} (Pope 2000; Girimaji 2000). Pressure is also essential for understanding and modeling cavitation^{4,5} (Arndt 2002; Brennen 1995).

Because of the importance of the pressure information in flow field, and in recognition of the need of a reliable tool for instantaneous spatial pressure distribution measurements, efforts in developing non-intrusive pressure measurement techniques have been carried out in the past decade in the fluids community. It is shown that the instantaneous pressure distribution in an incompressible turbulent flow field can be reconstructed by integration of the measured material acceleration, which constitutes the dominant contributor to pressure gradient with the viscous term being negligible for flows at high Reynolds number and away from wall, as demonstrated by Liu and Katz⁶⁻⁹ (2003, 2006, 2008, 2013), van Oudheusden¹⁰ (2008), Ragni *et al.*¹¹ (2009) and Joshi *et al.*¹² (2014), to name a few. The material acceleration can be measured non-intrusively using PIV (Particle Image Velocimetry), either discretely⁶⁻⁸ or continuously^{9,12} time-resolved. Once the material acceleration is obtained, the pressure gradient is known. Further integrating it will obtain the pressure. So far there are three major types of integration methods, i.e., *direct line integration*, *Poisson equation* and *least-square reconstruction*, that have been introduced and developed for the pressure reconstruction from the measured material acceleration. For direct line integration, representative method is the so-called *Circular Virtual Boundary, Omni-Directional Integration*⁶⁻⁹ over the entire measurement domain, which was evolved recently to a new algorithm featuring *rotating parallel ray*¹³ as integration path guidance. Representative *Poisson equation* approach can be found in de Kat and van Oudheusden¹⁴⁻¹⁵ (2010, 2012), Violato *et al.*¹⁶ (2011), and Auteri *et al.*¹⁷ (2015), etc. Review and comparison of the *direct line integration* and *Poisson equation* pressure reconstruction approaches can be found in Charonko *et al.*¹⁸ (2010), and van Oudheusden¹⁹ (2013). The *least-square reconstruction* approach²⁰ (Jeon *et al.*, 2015) was recently used to experimentally obtain instantaneous pressure field in a wake of a separated flow over an airfoil. This approach was also referred to as *direct matrix inversion* by Liu and Katz⁷ (2006).

Besides the pressure reconstruction methods, one area that is important yet has not been investigated thoroughly is the effect of the PIV measurement resolution on the accuracy of the measured pressure. To accurately measure the pressure distribution in a turbulent flow field, the measurement probe volume, i.e., the PIV interrogation window size should be able to resolve the smallest length scale, i.e., the Kolmogorov length scale in the turbulence flow field. However, due to technical constraints, usually the spatial resolution of the digital PIV is at least one or two orders of magnitude larger than that of the smallest turbulence length scale in a turbulent flow field, depending on Reynolds number and PIV setup. The resolution issue becomes even more prominent for tomographic PIV, as its resolution is usually coarser than that of planar PIV. Because of the finite spatial resolution, the pressure reconstructed from PIV measurement is actually subjected to the effect of spatial filtering. Consequently, the reconstructed pressure is effectively imbedded with the contribution from the subgrid-scale stress, which is a term appearing in the filtered Navier-Stokes equation as a result of the spatial filtering imposed by the finite resolution of the PIV measurement.

To quantify the effect of the SGS stress on the accuracy of the non-intrusive spatial pressure measurement, we use box filtering to filter the pressure as well as the three dimensional velocity components of both the isotropic turbulence and the turbulent channel flow direct numerical simulation (DNS) data available to public from the John Hopkins University Turbulence Database (JHTDB) (Li *et al.*²¹, 2008, Perlman *et al.*²², 2007 and Graham *et al.*²³, 2013). As a way to simulate the pressure measurement process, we apply the material acceleration calculation and pressure reconstruction procedures introduced in Liu and Katz⁷⁻⁹ to obtain the pressure distribution. The reconstructed pressure, with and without the incorporation of the SGS stress, is compared with the pressure filtered directly from the DNS database, thus enabling quantification of the SGS stress influence on the reconstructed pressure. To compensate the SGS stress influence, the SGS stress term calculated using the similarity model²⁴ (Meneveau and Katz, 2000) is incorporated in the pressure reconstruction process based on the filtered velocity data. The effectiveness of the compensation is then gauged by comparison with the filtered DNS pressure.

Preliminary analysis of the *forced isotropic turbulence* based on a $5 \times 5 \times 5$ box filter with 50% planar overlap²⁵ (Liu *et al.*, 2015) shows that although at most areas the magnitude of the SGS stress tensor is far less than that of the pressure gradient, at certain locations in the flow field, the SGS stress differential terms actually have dominant values that dwarf the pressure gradient, suggesting the neglect of the SGS stress term in the pressure reconstruction process is not appropriate, even for isotropic flow field. The analysis also confirms that the neglect of the viscous term results

in a negligible changes in the reconstructed pressure for the isotropic turbulence. However, as a contrast, the neglect of the SGS stress term results in a significant increase in both the bias error and the random error, suggesting the SGS term must be accounted for in the PIV pressure measurement. The random error in the reconstructed instantaneous pressure caused by the SGS stress is about 4.4% of the r.m.s. fluctuation of the filtered isotropic pressure. Correction using similarity SGS stress modeling reduces the error to 2.1%, confirming the benefit of the error compensation method.

In this paper, we focus on reporting the investigation result of resolution analysis based on the *DNS channel flow* data. Since large shear stress near the channel wall region is involved in the data analysis, this turbulence channel flow investigation represents a more practical and more challenging test case in comparison with the isotropic turbulence data. The resolution effect on the accuracy of the reconstructed pressure due to neglect of SGS stress for the channel shear flow will be characterized, and the effectiveness of the compensation method based on SGS similarity modelling will be presented. It is anticipated that the compensation method will bring in positive impact on the practice of non-intrusive volumetric spatial pressure measurement in the fluid dynamics community.

The paper will be arranged as follows: In section II, the JHU channel flow turbulence database will be briefly reviewed. Subsequently in section III, the governing equations for the forced turbulent channel flow will be listed. The method of investigation of the present work will be described in Section IV. Results and discussion will be presented in Section V.

II. The JHU Channel Flow Turbulence Database

The JHU turbulent channel flow database is attained via direct numerical simulation (DNS) of wall bounded flow. Periodic boundary conditions are imposed in the longitudinal and traverse directions, and no-slip conditions along the top and bottom walls. When producing the data from DNS, the Navier-Stokes equations are solved with a wall-normal, velocity-vorticity formulation²⁶ (Kim, *et al.*, 1987). The turbulent channel flow simulation uses the petascale DNS channel flow code developed at the University of Texas at Austin by Prof. Robert Moser's research group²⁷. Incompressible Navier-Stokes equations are solved using the pseudo-spectral (Fourier-Galerkin) method in wall-parallel (x, z) planes, and the 7th-order B-spline collocation method in the wall-normal (y) direction. Pressure is decoupled from the governing equations in the wall-normal, velocity-vorticity formulation. To obtain the pressure field for the database the pressure solves the pressure Poisson equation in the form

$$\nabla^2 p = -\frac{\partial u_i}{\partial x_j} \frac{\partial u_j}{\partial x_i} \quad (1)$$

where p is the *kinematic pressure*, i.e., the pressure divided by the constant density ρ_0 , and u_i represents the i -th velocity component using index notation. The Neumann boundary condition is of the form

$$\frac{\partial p}{\partial y} = \nu \frac{\partial^2 v}{\partial y^2} \quad (2)$$

where ν is the molecular kinematic viscosity and v the wall-normal velocity present at the top and bottom walls of the bounded channel. *This calculation is performed independently from the velocity field solution when outputting fields.* The simulation solves an approximate single flow through time, storing 3 component velocity vector and pressure fields every 5 time steps, yielding a time interval dt of 0.0065 between 4000 frames of instant realizations. The time interval between stored samples is smaller than the Kolmogorov time scale of 0.0446, thus rendering fully-resolved temporal scales for the simulated channel flow turbulence²⁷.

The simulation was performed on a three dimensional periodic grid with $2048 \times 512 \times 1536$ nodal points in physical space over a domain of $8\pi \times 2 \times 3\pi$ in x, y, z coordinate directions, yielding spatial intervals of 0.01227, 0.00391, 0.00614 in x, y, z coordinate directions, respectively, in the stored database samples. The grid size in the y direction are on the same order of the viscous length scale of 0.001 (Graham, *et al.*, 2013)²⁷.

III. The Governing Equations

The forced channel flow obtained by DNS is governed by the following momentum equation:

$$\frac{\partial u_i}{\partial t} + u_j \frac{\partial u_i}{\partial x_j} = -\frac{\partial}{\partial x_j} [p \delta_{ij}] + \nu \frac{\partial^2 u_i}{\partial x_j^2} + f \quad (3)$$

where t is time, f the forcing term, δ_{ij} the Kronecker delta for index notation. Correspondingly, the filtered momentum equation takes the form

$$\frac{\partial \tilde{u}_i}{\partial t} + \tilde{u}_j \frac{\partial \tilde{u}_i}{\partial x_j} = -\frac{\partial}{\partial x_j} [\tilde{p} \delta_{ij} + \tau_{ij}] + \nu \frac{\partial^2 \tilde{u}_i}{\partial x_j^2} + \tilde{f} \quad (4)$$

where “ $\tilde{\cdot}$ ” denotes filtering at a filter size of Δ . The sub-grid scale stress τ_{ij} is defined as

$$\tau_{ij} = \tilde{u}_i \tilde{u}_j - \tilde{u}_i \tilde{u}_j \quad (5)$$

which is a new quantity introduced as a result of filtering. In equation (4), $\frac{\partial \tilde{u}_i}{\partial t} + \tilde{u}_j \frac{\partial \tilde{u}_i}{\partial x_j}$ represents the material acceleration term, $-\frac{\partial}{\partial x_j} [\tilde{p} \delta_{ij}]$ the pressure gradient term, $-\frac{\partial \tau_{ij}}{\partial x_j}$ the SGS stress term, $\nu \frac{\partial^2 \tilde{u}_i}{\partial x_j^2}$ the viscous term, and \tilde{f} the forcing term.

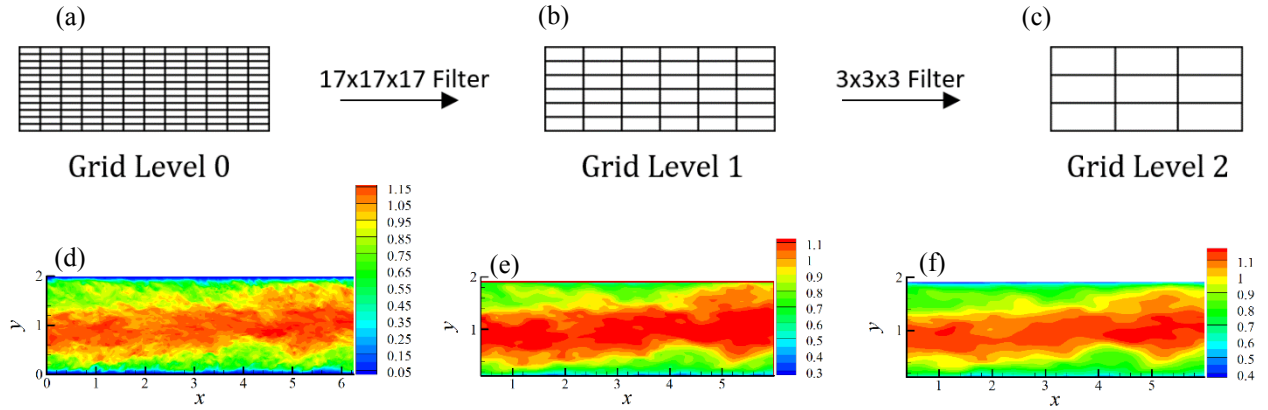


Figure 1. Three grid levels utilized in the application of the SGS stress modeling. (a) Grid Level 0 denotes the grid resolution level of the DNS data from the Johns Hopkins Turbulence Database; (b) Grid Level 1 is representative of the PIV measurement resolution, after an arbitrary $17 \times 17 \times 17$ filtering applied to DNS data; (c) Grid Level 2 represents the resolution after a $3 \times 3 \times 3$ filtering performed on data at Grid Level 1; (d) The unfiltered DNS u-velocity magnitude contour on Grid Level 0, (e) The filtered u-velocity magnitude contour on Grid Level 1, (f) The u-velocity magnitude contour after the second spatial filtering on Grid Level 2.

IV. Method of Investigation

A series of 1400 consecutive realizations of sample block data with $512 \times 512 \times 49$ grid nodal points were selected from the JHTDB channel flow DNS database for investigation. To simulate the PIV filtering effect, the velocity components and the pressure in the $512 \times 512 \times 49$ selected domain, denoted as Grid Level 0 in Figure 1, are spatially filtered using a $17 \times 17 \times 17$ box average with a 50% planar overlap, reducing the resolution of the cutout to a block of $62 \times 62 \times 5$ coarse nodal points (denoted as Grid Level 1 in Figure 1). By applying this $17 \times 17 \times 17$ box filtering, the data resolution in wall normal direction is spatially reduced to 16×0.00391 , which is roughly 62.6 times of the viscous length scale of the turbulent channel flow. Thus the data on Grid Level 1 can be approximated to represent a coarse resolution level of PIV measurement.

On Grid Level 1, the resolved SGS stress can be determined as

$$\tau_{ij}^{(1)} = \tilde{u}_i \tilde{u}_j - \tilde{u}_i \tilde{u}_j \quad (6)$$

However, for real PIV measurements, only the velocity of the flow is measured and the resolved SGS stress $\tau_{ij}^{(1)}$ is unknown. The SGS stress on the PIV resolution is what we seek to evaluate so as to be able to close the equation. Therefore, we use an approximation on a coarser resolution in conjunction with an appropriate scheme of SGS modeling to quantify the unknown SGS stress value. To do so, the data on Grid Level 1 is again filtered with a $3 \times 3 \times 3$ box filter, reducing the size of the now twice filtered data to $60 \times 60 \times 3$ nodal points. On this scale, the SGS stress $\tau_{ij}^{(2)}$ is defined as

$$\tau_{ij}^{(2)} = \tilde{\tilde{u}}_i \tilde{\tilde{u}}_j - \tilde{\tilde{u}}_i \tilde{\tilde{u}}_j \quad (7)$$

where “ $\tilde{\tilde{\cdot}}$ ” represents the second filtering of the data from Grid Level 1. Using SGS stress modeling, $\tau_{ij}^{(2)}$ can be related to $\tau_{ij}^{(1)}$, thus quantifying the SGS stress from the PIV data. The similarity SGS stress modeling²⁴ (Katz and Meneveau, 2000) is applied in this study due to the simplicity of the technique and its easily interpreted physical foundation. The basis of the SGS model is that the velocity field on the small scales (below the filter size Δ) behaves similarly to that on the larger scales (above Δ). Accordingly $\tau_{ij}^{(1)}$ at the PIV resolution on Grid Level 1 must be similar to $\tau_{ij}^{(2)}$, a stress tensor constructed from the resolved velocity field. Thus, the SGS stress model $\tau_{ij}^{(1)}$ can be quantified by

$$\tau_{ij_model}^{(1)} = C_{sim} \tau_{ij}^{(2)} \quad (8)$$

where C_{sim} is the modeling constant²⁴, which is chosen as 1.0 for the current application. The modeled SGS stress, $\tau_{ij_model}^{(1)}$ from Equation (8), can be used to close the filtered momentum equation and investigate the effectiveness of inclusion of the modeled SGS stress term on the accuracy improvement of the measured pressure.

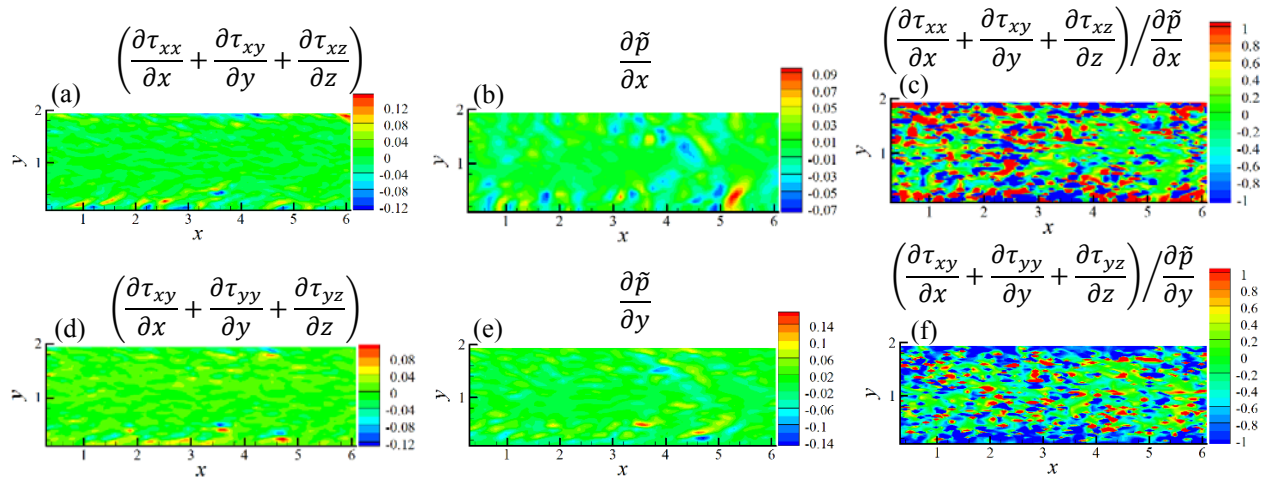


Figure 2. Comparison of the differential subgrid-scale stress terms with the corresponding gradients of the filtered DNS pressure using an arbitrary instant realization as an example.

With the resolved velocity component (u, v, w) and pressure (p) provided by the JHTDB, all terms in Equation (4) are known after the application of the first filtering except for the forcing term \tilde{f} . The forcing term \tilde{f} can be determined indirectly through balancing of Equation (4). The components of Equation (4), with or without the addition of the SGS stress term, can be spatially integrated respectively using the pressure reconstruction code developed by Liu and Katz⁶⁻⁹. The results of the integration can then be compared with the filtered DNS pressure, which can be considered as the “true pressure” that the nonintrusive PIV pressure measurement aims to capture at the PIV resolution level. By doing

so, the influence of the SGS term on the accuracy of the pressure measurement can be quantified. Strategic inclusion and exculsion of individual terms such as the viscous term can measure their contribution to the pressure measurement as well.

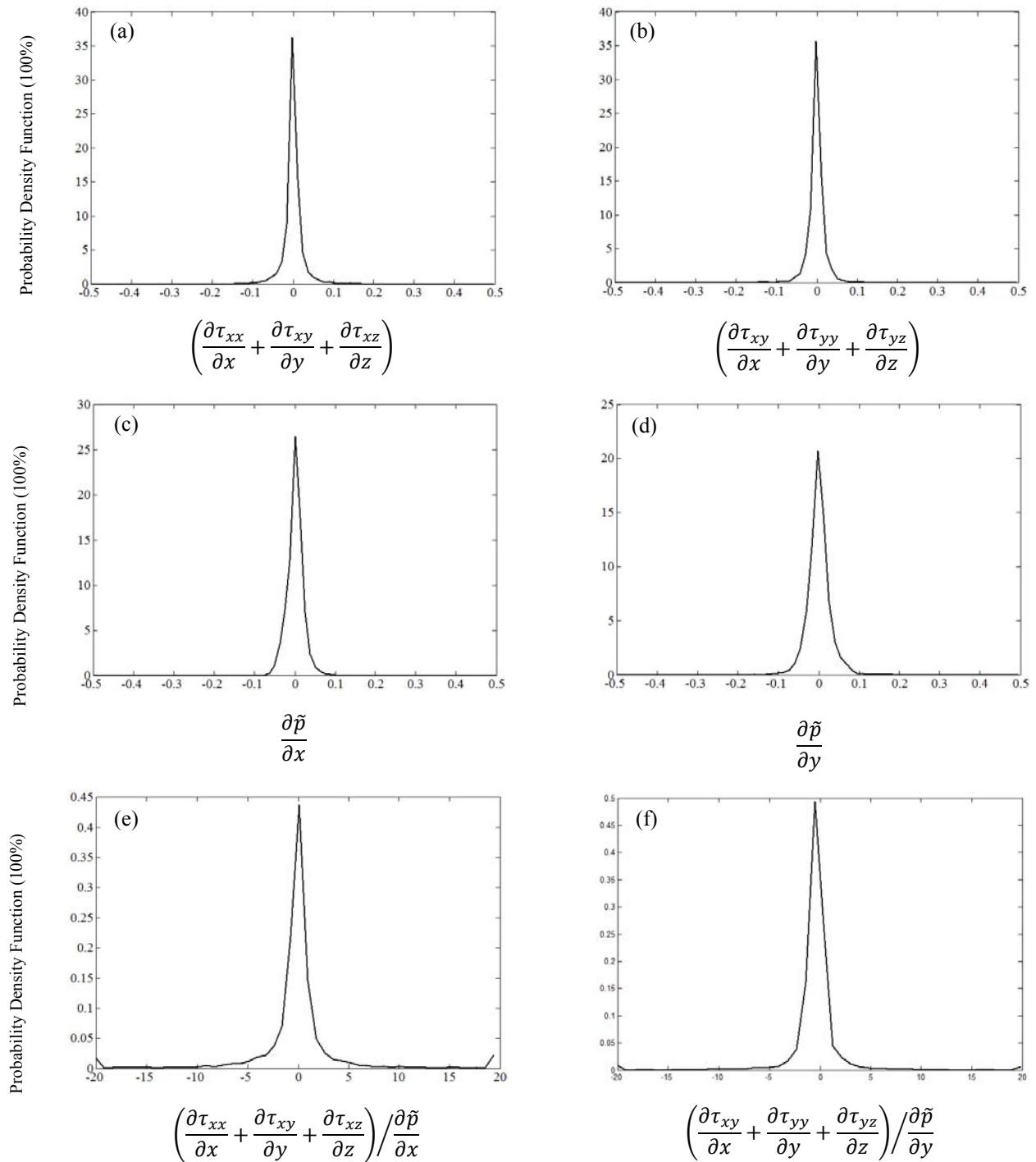


Figure 3. Probability density functions for the SGS term, the gradients of the filtered pressure and their ratios at the center plane of the $62 \times 62 \times 5$ domain of Grid Level 1.

V. Results and Discussion

The goal of this investigation is to determine the influence of the SGS stress on the accuracy of PIV pressure measurements in a wall bounded channel flow. We begin this inquiry by examining the relative magnitude of the SGS stress tensor in comparison with the gradients of the filtered pressure terms. The x - and y -components of the SGS stress term, pressure gradients and their corresponding ratio on the center plane of the $62 \times 62 \times 5$ field of Grid Level 1 using an arbitrary instant realization as an example are presented in Figure 2. Evident from Figure 2(a), (b), (d) and (e), the peak values of the SGS term occur near the channel wall, with magnitudes comparable with that of the corresponding pressure gradients. In contrast, in regions away from the wall, the SGS term is generally smaller. However, distributions of the ratio between the two quantities shown in Figures 2(c) and (f) indicate that certain isolated regions exist where the SGS stress is considerably larger than that of the pressure gradients. This qualitative understanding is further confirmed by the probability density function (pdf) distributions and the associated statistics of these two types of terms, as shown in Figure 3 and Table 1, respectively.

Table 1. Statistics of the SGS stress term, the pressure gradients and their ratios at the center plane of a sample $62 \times 62 \times 5$ course domain of Grid Level 1.

	Mean	Standard Deviation, σ	Kurtosis, k	Kurtosis/ Standard Deviation, k/σ
$\left(\frac{\partial \tau_{xx}}{\partial x} + \frac{\partial \tau_{xy}}{\partial y} + \frac{\partial \tau_{xz}}{\partial z}\right)$	2.507E-04	2.335E-02	12.05	516.2
$\left(\frac{\partial \tau_{xy}}{\partial x} + \frac{\partial \tau_{yy}}{\partial y} + \frac{\partial \tau_{yz}}{\partial z}\right)$	-8.043E-04	1.857E-02	9.946	535.5
$\frac{\partial \tilde{p}}{\partial x}$	5.853E-04	1.020E-02	4.788	469.4
$\frac{\partial \tilde{p}}{\partial y}$	-8.991E-05	2.694E-02	6.458	240.1
$\left(\frac{\partial \tau_{xx}}{\partial x} + \frac{\partial \tau_{xy}}{\partial y} + \frac{\partial \tau_{xz}}{\partial z}\right) / \frac{\partial \tilde{p}}{\partial x}$	0.4744	25.67	1020.6	39.76
$\left(\frac{\partial \tau_{xy}}{\partial x} + \frac{\partial \tau_{yy}}{\partial y} + \frac{\partial \tau_{yz}}{\partial z}\right) / \frac{\partial \tilde{p}}{\partial y}$	-1.031	32.28	2829.6	87.65

Clearly visible in Figure 3 and Table 1, all the pdf profiles of these quantities are close to being symmetric with respect to their almost zero mean values. However, the pdf distributions of both the x and y components of the SGS stress differential and pressure gradient terms (Figure 3a, b, c and d) are all strongly “outlire”-prone, as evidenced by their high kurtosis numbers ($\sim O(100\sigma)$, Table 1), indicating that their pdf profile shape is strongly deviated from that of the Gaussian distribution, for which the kurtosis value is 3σ . This strong “outlire”-prone behavior is due to the high wall shear effect near the channel wall. Evident in Figure 3(e) and (f) and Table 1, the large standard deviation (~ 20 - 30) and extremely high kurtosis (~ 1021 - 2830) of the ratio between the SGS stress differential term and the pressure gradient, indicates that at certain locations in the filtered flow field, the SGS stress differential terms have a dominant value that dwarfs the local pressure gradient, implying that neglecting the SGS term would introduce error to the reconstructed pressure if it is not appropriately accounted for. To quantify the influence of the SGS stress term on the accuracy of the reconstructed pressure, we resort to comparisons of the integral results of the different terms that comprise Equation (4).

Figure 4 shows the comparisons of the integral results of the viscous, forcing, SGS stress, and material acceleration terms with the filtered pressure at Grid Level 1 as well as the unfiltered DNS pressure. The integration is achieved using the pressure reconstruction code developed by Liu and Katz⁶⁻⁹, based on *circular virtual boundary, omnidirectional integration method*. The forcing term is obtained from the balance of Equation (4) as

$$\iint_{x-y \text{ plane}} \tilde{f} = \iint_{x-y \text{ plane}} \left(\frac{\partial \tilde{u}_i}{\partial t} + \tilde{u}_j \frac{\partial \tilde{u}_i}{\partial x_j} + \frac{\partial}{\partial x_j} [\tilde{p} \delta_{ij} + \tau_{ij}] - \nu \frac{\partial^2 \tilde{u}_i}{\partial x_j^2} \right) \quad (9)$$

As shown in Figure 4, peak values of both the viscous and the SGS stress terms occur near the channel wall, and have the same order of magnitude as those of the material acceleration and the filtered pressure. In regions away from the wall, besides the forcing term, the material acceleration term is shown to have a dominant contribution to pressure in comparison with the viscous and the SGS stress terms. The vital inclusion of the SGS stress and viscous terms near the channel wall represent a more practical and more challenging test case in comparison with the isotropic turbulence case²⁵ where the viscous term was negligible.

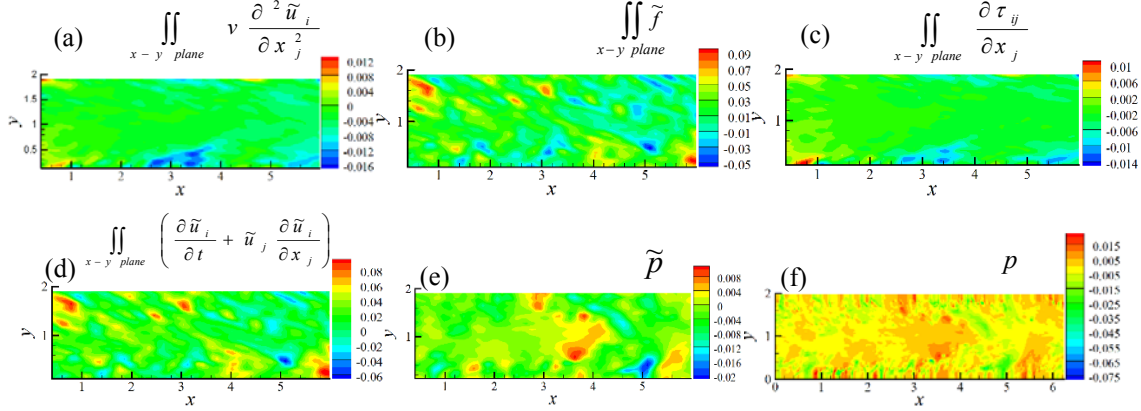


Figure 4. Comparison of the integral results of (a) viscous, (b) forcing, (c) SGS stress, and (d) material acceleration terms with (e) the filtered pressure and (f) the unfiltered DNS pressure using an arbitrary instant realization as an example.

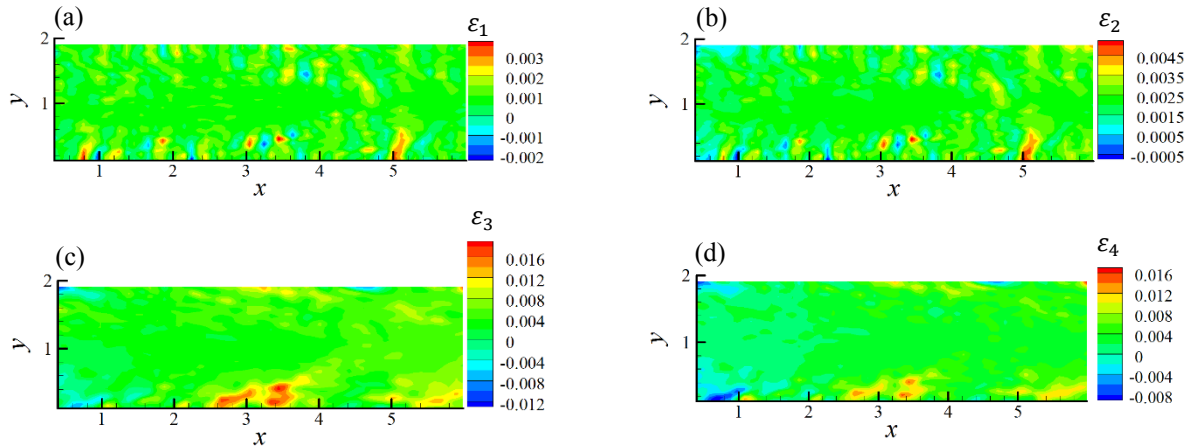


Figure 5. Comparison of the differences between the reconstructed pressure at different levels of approximation and the filtered pressure \tilde{p} using an arbitrary instant realization as an example. (a), all terms accounted for; (b), viscous term only is neglected; (c), SGS stress term only is neglected and (d), SGS stress term is substituted with the modeled SGS stress based on similarity modeling.

To further gauge the effect of different levels of approximation of the pressure gradient on the accuracy of the pressure reconstruction, and to evaluate the effect of similarity modeling on the compensation of the errors due to lack of resolved SGS stress, we define the following error quantities, with the filtered pressure \tilde{p} treated as the “true pressure” value that the PIV measurement aims to capture.

$$\epsilon_i = \iint_{x-y \text{ plane}} \left(\underbrace{\frac{\partial \tilde{u}_i}{\partial t}}_{\text{Material Acceleration}} + \underbrace{\tilde{u}_j \frac{\partial \tilde{u}_i}{\partial x_j}}_{\text{SGS Stress}} + \underbrace{\frac{\partial \tau_{ij}}{\partial x_j}}_{\text{Viscous}} - \underbrace{\nu \frac{\partial^2 \tilde{u}_i}{\partial x_j^2}}_{\text{Viscous}} - \underbrace{\tilde{f}}_{\text{Forcing}} \right) - \underbrace{\tilde{p}}_{\text{Filtered Pressure}} \quad (10)$$

$$\varepsilon_2 = \iint_{x-y \text{ plane}} \left(\underbrace{\frac{\partial \tilde{u}_i}{\partial t} + \tilde{u}_j \frac{\partial \tilde{u}_i}{\partial x_j}}_{\text{Material Acceleration}} + \underbrace{\frac{\partial \tau_{ij}}{\partial x_j}}_{\text{SGS Stress}} - \underbrace{\tilde{f}}_{\text{Forcing}} \right) - \tilde{p} \quad (11)$$

$$\varepsilon_3 = \iint_{x-y \text{ plane}} \left(\underbrace{\frac{\partial \tilde{u}_i}{\partial t} + \tilde{u}_j \frac{\partial \tilde{u}_i}{\partial x_j}}_{\text{Material Acceleration}} - \underbrace{\nu \frac{\partial^2 \tilde{u}_i}{\partial x_j^2}}_{\text{Viscous}} - \underbrace{\tilde{f}}_{\text{Forcing}} \right) - \tilde{p} \quad (12)$$

$$\varepsilon_4 = \iint_{x-y \text{ plane}} \left(\underbrace{\frac{\partial \tilde{u}_i}{\partial t} + \tilde{u}_j \frac{\partial \tilde{u}_i}{\partial x_j}}_{\text{Material Acceleration}} + \underbrace{\frac{\partial \tau_{ij}^{(1)} \text{-model}}{\partial x_j}}_{\text{Modeled SGS Stress}} - \underbrace{\nu \frac{\partial^2 \tilde{u}_i}{\partial x_j^2}}_{\text{Viscous}} - \underbrace{\tilde{f}}_{\text{Forcing}} \right) - \tilde{p} \quad (13)$$

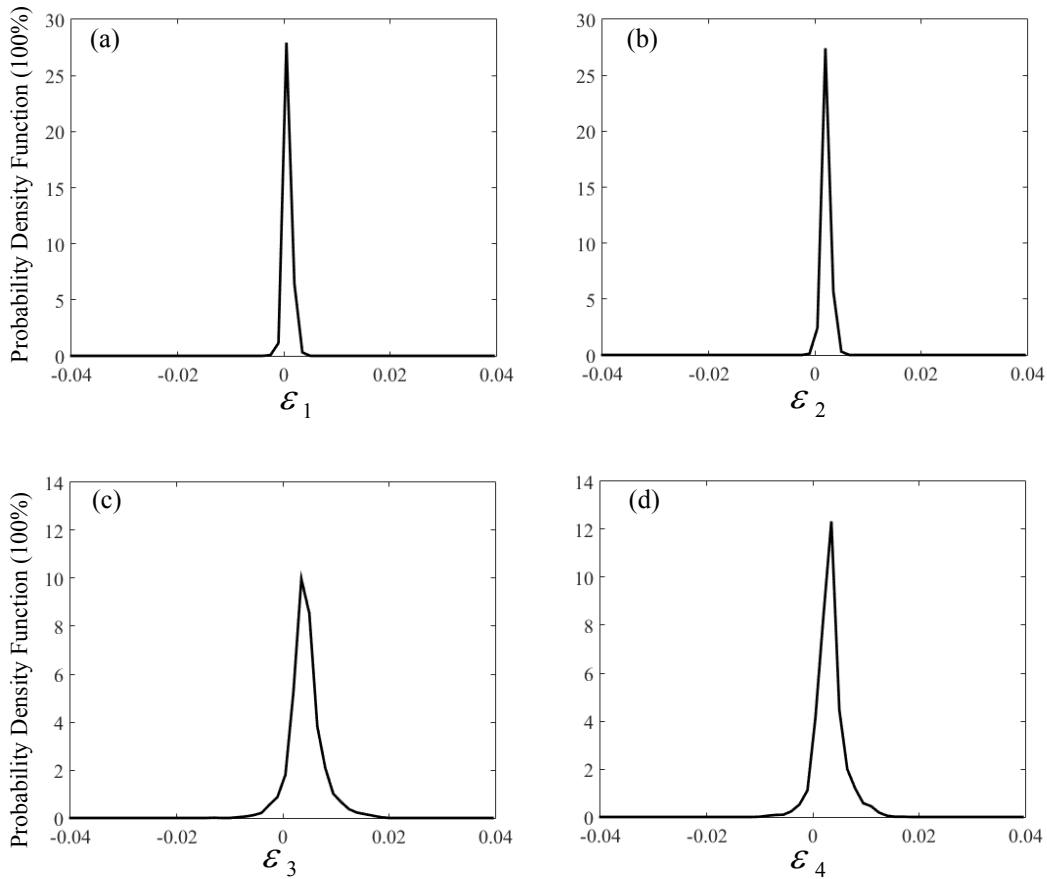


Figure 6. Probability density function of the differences between the reconstructed pressure at different levels of approximation and the filtered pressure \tilde{p} , using an arbitrary instant realization as an example. (a), all terms accounted for; (b), viscous term neglected; (c), SGS stress term neglected; and (d), the unknown SGS stress is substituted with the modeled SGS stress based on similarity modeling.

As defined in the above equations, ε_1 is the error of the integral in which all terms of the filtered momentum equation, Equation (4), including material acceleration, SGS stress, viscous and forcing are accounted for to approximate the filtered pressure gradient. As the best possible accuracy, ε_1 represents the “baseline” error which other quantities can compare with. In contrast, ε_2 is used to examine the error due to the omission of the viscous term,

while ε_3 to examine the effect of neglecting the SGS term, and ε_4 to examine the effect of substituting the unavailable SGS stress term with the modeled SGS stress, i.e., $\tau_{ij,model}^{(1)} = C_{sim}\tau_{ij}^{(2)}$ in pressure reconstruction.

The distributions of the above errors are shown in Figure 5. The contributing sources to the baseline ε_1 mainly include a variety of numerical errors accumulated from different steps on the calculation procedures before obtaining the final integrals. The error ε_2 shown in Figure 5(b) indicates that the omission of the viscous term introduces a small but noticeable error in comparison with Figure 5(a). However, the neglect of the SGS stress term, shown in Figure 5(c), yields a significant error increase in comparison with ε_1 . Using the previously defined similarity model to substitute the unknown SGS stress obviously improves the situation in comparison to ε_3 , as demonstrated clearly by ε_4 in Figure 5(d).

To further quantify these errors, pdf plots of these errors based on a single instantaneous realization are presented in Figure 6. Related statistics, averaged over 1400 realizations are shown in Table 2. The standard deviation of the fluctuating filtered pressure $\sigma_{\tilde{p}}$ is used to gauge (normalize) the statistics. As the statistics in Table 2 reveals the neglect of the viscous term (ε_2) introduced a small amount of error into the pressure reconstruction, but still on the same order of magnitude as the baseline error ε_1 . This agrees with the comparison of Figures 5 (a) and (b) and Figures 6 (a) and (b). Consistent with the previously visualized results, neglecting the SGS stress, ε_3 , increases both the bias error (i.e. mean value of error normalized by $\sigma_{\tilde{p}}$) from 1.77% to -36.63% and the random error (i.e., standard deviation of error normalized by $\sigma_{\tilde{p}}$) from 17.30% to 106.29%. Similarity modeling using Grid Level 2 approximation to substitute the unknown SGS stress improves the situation by reducing the magnitude of bias error and random error to 10.77% and 80.38% respectively, as seen in Table 2. The improvement of the error by inclusion of the model SGS stress confirms our hypothesis and supports the motivation to include the modeled SGS when reconstructing pressure. Note that in PIV pressure measurement, the bias error may be corrected by offset of the measured mean pressure using a reference pressure. The large random error ($\sim 100\%$) due to the omission of the SGS stress occurring at $17\times 17\times 17$ filtering level also indicates the need of sufficient measurement resolution in ensuring pressure reconstruction accuracy.

Table 2. Statistics of pressure differences averaged over 1400 instantaneous realizations

	All terms accounted for, ε_1	Viscous term neglected, ε_2	SGS stress term neglected, ε_3	SGS stress based on similarity modeling, ε_4
Mean $\varepsilon / \sigma_{\tilde{p}}$	0.0177	0.4055	-0.3663	.1077
Standad Deviation $\varepsilon / \sigma_{\tilde{p}}$	0.1730	0.2037	1.0629	0.8038

Note: $\sigma_{\tilde{p}} = 0.0028$

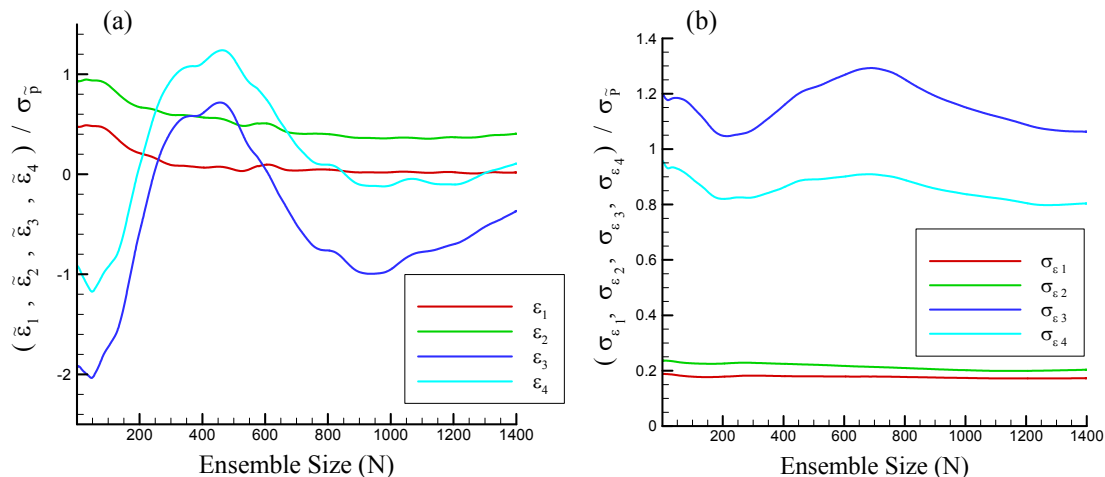


Figure 7. Convergence of (a) the mean and (b) the standard deviation of the pressure errors averaged over 1400 consecutive instantaneous realizations.

The simulation of turbulent channel flow was performed over 1400 instantaneous in order to obtain a converged accepted result. The progression of the convergence of the bias error and random error are presented in Figure 7 (a)

and (b), respectively. It seems that with the 1400 ensemble size, all of the standard deviations of errors ε_1 through error ε_4 reach convergence. However, the mean values of errors ε_3 and errors ε_4 still oscillates even with the 1400 ensemble size.

VI. Conclusion and future work

The effect of the SGS stress on the accuracy of the non-intrusive spatial pressure measurement is investigated using data from a direct numerical simulation of turbulent channel flow available to the public at the John Hopkins University Turbulence Database (JHTDB). A series of 1400 consecutive realizations of sample block data with $512 \times 512 \times 49$ grid nodal points were selected. To simulate the PIV filtering effect, these data are spatially filtered using a $17 \times 17 \times 17$ box average with a 50% planar overlap, giving rise to PIV resolution of roughly 62.6 times of the viscous length scale of the turbulent channel flow.

Examination of the relative magnitude of the SGS stress tensor components against their corresponding pressure gradient terms shows that although at most areas the magnitude of the SGS stress tensor is less than that of the pressure gradient, at certain locations in the flow field, especially near the channel walls, neglecting the SGS stress term in the pressure reconstruction process may not be appropriate.

Comparison of the reconstructed pressure at different levels of pressure gradient approximation with the filtered pressure shows that the neglect of the viscous term results in a small but noticeable change in the reconstructed pressure, suggesting that due to the presence of wall bounds in the flow the viscous term should be included for desired accuracy, especially in regions near channel walls. However, as a contrast, the neglect of the SGS stress results in a more significant increase in both the bias error and random error, indicating the SGS term need to be accounted for in the PIV pressure measurement. Correction using similarity SGS modeling reduces the random error from 106.29% to 80.38% of the r.m.s. fluctuation of the filtered pressure, confirming the benefit of the error compensation method.

The large error ($\sim 100\%$) due to the omission of the SGS stress occurring at $17 \times 17 \times 17$ filtering level indicates the need of sufficient measurement resolution in ensuring pressure reconstruction accuracy. To demonstrate that anticipated positive effect of resolution increase on the improvement of the pressure reconstruction accuracy, the same data set will be filtered with a smaller $5 \times 5 \times 5$ filter (corresponding to 15.6 times of the viscous length scale, a more realistic PIV resolution), and the procedures and analyses outlined in this paper will be implemented, as the ongoing and future work. In addition, effects of using different SGS stress modeling methods, such as dynamic and Smagorinsky modeling, in suppressing the pressure reconstruction error will be investigated.

Acknowledgments

This project is funded by the San Diego State University Research Foundation. The help from Prof. Charles Meneveau and Mr. Stephen Hamilton of Johns Hopkins University in retrieving the channel flow turbulent data from the JHTDB is gratefully acknowledged.

References

- ¹Blake, W.K., *Mechanics of Flow-Induced Sound and Vibration*, Academic, New York, 1986.
- ²Pope, S.B., *Turbulent Flows*, Cambridge University Press, Cambridge, 2000.
- Periodicals*
- ³Girimaji, S.S., "Pressure-Strain Correlation Modeling of Complex Turbulent Flows", *J. Fluid Mech.*, Vol. 422, November 2000, pp.91-123.
- ⁴Arndt, R. E. A., "Cavitation in vortical flows," *Annu. Rev. Fluid Mech.* 34, 143, January 2002.
- ⁵Brennen, C. E., *Cavitation and bubble dynamics*, Oxford University Press, Oxford, 1995.
- ⁶Liu, X. and Katz, J., "Measurements of Pressure Distribution by Integrating the Material Acceleration", Cav03-GS-14-001, *Proc. of the 5th International Symposium on Cavitation (Cav2003)*, Osaka, Japan, Nov. 1-4, 2003.
- ⁷Liu, X. and Katz, J., "Instantaneous Pressure and Material Acceleration Measurements using a Four Exposure PIV System," *Exp. Fluids*, Vol. 41, No. 2, August 2006, pp227-240.
- ⁸Liu, X. and Katz, J., "Cavitation Phenomena Occurring due to Interaction of Shear Layer Vortices with the Trailing Corner of a 2D Open Cavity," *Physics of Fluids*, Vol. 20, No. 4, April 2008, 041702, DOI:10.1063/1.2897320.
- ⁹Liu, X. and Katz, J., "Vortex-Corner Interactions in a Cavity Shear Layer Elucidated by Time Resolved Measurements of the Pressure Field," *J. Fluid Mech.*, Vol. 728, August 2013, pp 417-457. DOI: 10.1017/jfm.2013.275.
- ¹⁰Van Oudheusden BW, 2008, "Principles and application of velocimetry-based planar pressure imaging in compressible flows with shocks", *Exp. Fluids* 45, 657-674.

- ¹¹Ragni, D., Ashok, A., Van Oudheusden, B. W. and Scarano, F., “Surface Pressure and Determination of a Transonic Aerofoil Based on Particle Image Velocimetry,” *Meas. Sci. Technol.*, Vol. 20, No. 7, July 2009, 074005.
- ¹²Joshi, P., Liu, X. and Katz, J., Effect of mean and fluctuating pressure gradients on boundary layer turbulence, *Journal of Fluid Mechanics*, Vol. 748, June 2014, pp. 36–84. DOI:10.1017/jfm.2014.147.
- ¹³Liu, X., Moreto, J. R. and Siddle-Mitchel, S., Instantaneous Pressure Reconstruction from Measured Pressure Gradient using Rotating Parallel Ray Method, AIAA-2016-1049, 54th AIAA Aerospace Sciences Meeting, AIAA SciTech, Jan. 2016, doi: 10.2514/6.2016-1049.
- ¹⁴De Kat, R. and Van Oudheusden, B. W., “Instantaneous planar pressure from PIV: analytic and experimental test-cases”. In *15th International Symposium on Applications of Laser Techniques to Fluid Mechanics*, Lisbon, Portugal, July 5-8, 2010.
- ¹⁵De Kat, R. and Van Oudheusden, B. W. “Instantaneous planar pressure determination from PIV in turbulent flow”, *Exp Fluids* Vol. 52, No. 5, pp. 1089–1106, May 2012.
- ¹⁶Violato, D., Moore, P. and Scarano, F., “Lagrangian and Eulerian Pressure Field Evaluation of Rod-Airfoil Flow from Time-Resolved Tomographic PIV”, *Exp. Fluids.*, Vol.50, No. 4, April 2011, pp. 1057–1070.
- ¹⁷Auteri, F., Carina, M., Zangaglia, D., Montagnon, D., Libertine, G., Mars, C. B. and Zanetti, A., “A Novel Approach for Reconstructing Pressure from PIV Velocity Measurements,” *Exp Fluids*, Vol, 56 , No.45, February 2015, DOI 10.1007/s00348-015-1912-z.
- ¹⁸Charonko, J. J., King, C. V., Smith, B. L. and Vlachos, P. P., “Assessment of Pressure Field Calculations from Particle Image Velocimetry Measurements,” *Meas. Sci. Technol.*, Vol. 21, No.10, October 2010, 105401.
- ¹⁹Van Oudheusden, B. W., “PIV-based pressure measurement,” *Meas. Sci. Technol.* Vol. 24, No.3, March 2013, 032001.
- ²⁰Jeon, Y.J., Chatellier, L., Beaudoin, A., and David, L., “Least-square reconstruction of instantaneous pressure field around a body based on a directly acquired material acceleration in time-resolved PIV”, *11th International Symposium on Particle Image Velocimetry – PIV15*, Santa Barbara, California, September 14-16, 2015.
- ²¹Li Y, Perlman E, Wan M, Yang Y, Meneveau C, Burns R, Chen S, Szalay A and Eyink G, “A public turbulence database cluster and applications to study Lagrangian evolution of velocity increments in turbulence”, *J of Turbulence*. Vol. 9, No. 31, January 2008, pp. 1-29.
- ²²Perlman E, Burns R, Li Y and Meneveau C, 2007, “Data Exploration of Turbulence Simulations using a Database Cluster”, *Supercomputing SC07*, ACM, IEEE, 2007.
- ²³Graham, J., Lee, M., Malaya, N., Moser, R.D., Eyink, G., Meneveau, C., Kanov, K., Burns, R. and Szalay, A, 2013, “Turbulent channel flow data set”, available at <http://turbulence.pha.jhu.edu/docs/README-CHANNEL.pdf>.
- ²⁴Meneveau C and Katz J, 2000, “Scale-invariance and turbulence models of large-eddy simulation”, *Annu. Rev. Fluid Mech.*, 2000.
- ²⁵Liu, X., Siddle-Mitchel, S., Rybarczyk, R. and Katz, J., 2015, “Investigation of the influence of the subgrid-scale stress on non-intrusive spatial pressure measurement using an isotropic turbulence database”, *11th International Symposium on Particle Image Velocimetry – PIV15*, Santa Barbara, California, September 14-16, 2015.
- ²⁶Kim, J., Moin, P., and Moser R., “Turbulence statistics in fully developed channel flow at low Reynolds number”, *J. Fluid Mech.*, 177:133–166, 1987.
- ²⁷Lee, M., Malaya, N., and Moser, R. D., “Petascale direct numerical simulation of turbulent channel flow on up to 786k cores”, *Supercomputing (SC13)*, 2013.